Available online at www.sciencedirect.com

SCIENCE DIRECT®

Nuclear Instruments and Methods in Physics Research A 562 (2006) 298–305

NUCLEAR INSTRUMENTS & METHODS IN PHYSICS RESEARCH
Section A

www.elsevier.com/locate/nima

A novel Calorimeter Telescope for identification of relativistic heavy-ion reaction channels

R. Lozeva[a,b,*], J. Gerl[b], M. Górska[b], I. Kojouharov[b], S. Mandal[b,1], H.-J. Wollersheim[b], D. Balabanski[a,c,2], F. Becker[b], J. Grębosz[b,d], A. Banu[b,3], P. Bednarczyk[b,d], P. Doornenbal[b,e], H. Schaffner[b]

[a] *Faculty of Physics, University of Sofia "St. Kl. Ohridski", Dj. Bourchier blvd. 5, 1164-Sofia, Bulgaria*
[b] *Gesellschaft für Schwerionenforschung, Planckstrasse 1, D-64291 Darmstadt, Germany*
[c] *Dipartamento di Fisica, Università di Camerino, Via Madonna delle Carceri str. 9, 62032-Camerino, Italy*
[d] *The Henryk Niewodniczański Institute of Nuclear Physics, Radzikowskiego str. 152, 31342-Krakow, Poland*
[e] *Institut für Kernphysik, Universität zu Köln, Zülpicherstr. 77, D-50937, Cologne, Germany*

Received 4 October 2005; received in revised form 10 February 2006; accepted 19 February 2006
Available online 20 March 2006

Abstract

A novel Calorimeter Telescope (CATE) is employed in the fast beam Rare Isotope Investigations at GSI (RISING) γ-campaign with relativistic energies at the Fragment Separator (FRS) at GSI. CATE consists of nine modular Si$-$CsI(Tl) detector telescopes for position and $\Delta E - E_{\mathrm{res}}$ measurements. It registers the scattering angle and identifies the charge (Z) and the mass (A) of exotic heavy ions produced after secondary fragmentation or Coulomb excitation.

PACS: 29.40.Gx; 29.40.Mc; 29.40.Vj

Keywords: Tracking and position sensitive detectors; Scintillation detectors; Calorimeters

---

1. Introduction and motivation

The FRS facility [1] at GSI provides a unique opportunity to separate a variety of relativistic heavy-ion beams which are produced at a primary target and transported to a final focus, where a secondary target is located. The FRS allows an isotope separation using the Bρ-ΔE-Bρ technique [1] and an identification using a system of tracking detectors (see Fig. 1) before the secondary reaction target.

At this position the RISING [2] spectrometer is situated, utilizing fifteen of the ex-EUROBALL [3] Ge-Cluster detectors [4]. Within the first, "fast beam" phase, the RISING experiments aimed at γ-ray spectroscopy of secondary isotopes, produced in nucleon knockout and fragmentation reactions or relativistic Coulomb excitation at the secondary target, yielding unique nuclear structure information which cannot be obtained by other techniques.

In order to obtain information about the excited residues, channel selection after the reaction target is needed. Here, the energy loss (ΔE) combined with a residual energy (E_{res}) measurement, known as $\Delta E - E_{\mathrm{res}}$ method is favored for identification of the secondary reaction products and to measure their scattering angle (for kinematics reconstruction). Detector systems utilizing this type of energy measurement have shown a large and simple applicability in a wide range of experimental conditions in

---

[*] Corresponding author. Faculty of Physics, University of Sofia "St. Kl. Ohridski", Dj. Bourchier blvd. 5, 1164-Sofia, Bulgaria.
E-mail addresses: rady@phys.uni-sofia.bg, r.lozeva@gsi.de (R. Lozeva).

[1] Present address: University of Delhi, University Road, 110007-New Delhi, India.

[2] Present address: Institute of Nuclear Research and Nuclear Energy, Bulgarian Academy of Science, Tzarigradsko chaussee blvd. 72, 1784-Sofia, Bulgaria.

[3] Cyclotron Institute, Texas A&M University, College Station, TX 77843, MS#3366, USA.

0168-9002/$ - see front matter © 2006 Elsevier B.V. All rights reserved.
doi:10.1016/j.nima.2006.02.163

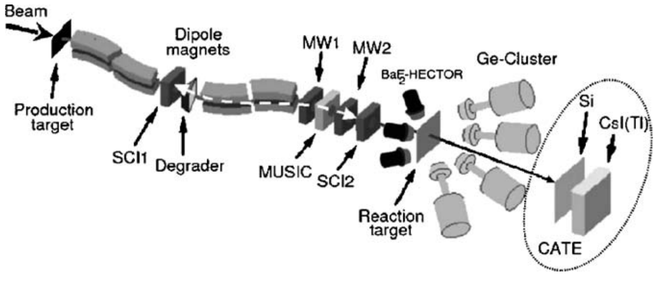

Fig. 1. Schematic layout of the RISING experimental setup for the fast beam campaign. The identification detectors consist of two Multi Wire detectors (MW1 and MW2) for position (x, y) measurement, an Ionization Chamber (MUSIC) for energy loss (respectively Z) measurement and two plastic scintillators (SCI1 and SCI2) for Time-of-Flight, ToF (respectively velocity β) measurement. The identification after the secondary target is performed with the new Calorimeter Telescope CATE.

many laboratories [5–12]. However, a $\Delta E - E_{\mathrm{res}}$ detector system has not been employed for a relativistic heavy-ion identification so far. The present paper reports on a novel calorimeter telescope constructed for this purpose. In order to design such a new system, several investigations have been performed for the selection of particle detectors for ΔE and E_{res} measurements. Based on these experimental studies, a new position sensitive $\Delta E - E_{\mathrm{res}}$ Calorimeter Telescope (CATE) [13] has been built, consisting of a Si and a CsI(Tl) detector arrays.

The position sensitive Si detector array measures the particle's (x, y) position and is used for the reconstruction of the scattering angle after the secondary target. From the energy loss, detected in the Si (ΔE) and CsI(Tl) (E_{res}) detectors, the ion charge Z and mass A are derived, respectively. The CATE detector system has been used within the RISING fast beam campaign for the detection of primary and secondary heavy ions from ^{53}V up to ^{132}Xe in the energy range between 90 and 400 A MeV (at the detectors) with instantaneous rates between 10^2 and 10^4 pps.

2. Calorimeter Telescope—CATE

CATE is a chessboard-like array of nine $\Delta E - E_{\mathrm{res}}$ telescopes. Each of them comprises a position sensitive Si-pin detector and a corresponding CsI(Tl) detector coupled to a photodiode [13]. It is placed 1.4 m downstream from the secondary target (see Fig. 1) in order to have sufficient angular coverage for impact parameter measurements in the relativistic Coulomb excitation reactions. Thus, the opening angles are $\theta \in [-3.2, 3.2]^\circ$ and $\phi \in [-180, 180]^\circ$. Taking into account the solid angle coverage of the detectors in the array (see Fig. 2(a,b)), the efficiency with respect to the incoming particles amounts to 92%.

2.1. CATE-Si array

Two types of Si-pin detectors have been used for the CATE-Si array. These are a Si-IPP type semiconductor (model: $IPP2D50x50-300-SPE$) [14] and a Si-PIPS[4] type semiconductor (model: $PF50x50-300EB-L$) [15]. They differ slightly by their thickness, and significantly, by the resistivity of the resistive layer.

Each Si-ΔE counter has a size of $(50 \times 50)\,\mathrm{mm}^2$ and a thickness of 0.30 mm (for the Si-IPP) and 0.32 mm (for the Si-PIPS). A resistive carbon layer with a sheet resistance of $1-2\,\mathrm{k\Omega/cm^2}$ (for the Si-IPP) and $4-5\,\mathrm{k\Omega/cm^2}$ (for the Si-PIPS) serves as a front contact. This layer is used as a charge divider with four contact electrodes at the four corners. By comparing the relative pulse heights, obtained at these four electrodes, the position is calculated (see Section 3). Each corner contact has in addition a resistor of $1-1.5\,\mathrm{k\Omega}$ (for the Si-IPP) and $1.5-1.6\,\mathrm{k\Omega}$ (for the Si-PIPS) to reduce nonlinearities in the position determination as described i.e. in Refs. [16,17]. All detectors are placed in separate frames with size $(54 \times 54)\,\mathrm{mm}^2$ and altogether on a motherboard, as shown in Fig. 2(a,c).

The energy, ΔE, deposited by the incident particle, is measured by the back-side contact and the signal is proportional to the total charge created. From the energy loss in the detector (ΔE), the charge Z of the impinging particle is obtained (see Section 5.1).

An α-test measurement with a ^{241}Am source revealed the intrinsic position resolution $(\Delta x, \Delta y)$ of these detectors. It is better than $(5 \times 5)\,\mathrm{mm}^2$ for the Si-IPP detectors and better than $(3 \times 3)\,\mathrm{mm}^2$ for the Si-PIPS detectors. The intrinsic energy resolution for 5.5 MeV α-particles stopped inside the detector is better than 1.5% (FWHM) for both Si types. In-beam, the intrinsic energy resolution of both Si types, acting as transmission detectors, is found to be about 2.0% (FWHM) with primary ^{86}Kr ions with an energy of 150 A MeV and ^{58}Ni ions with an energy of 120 A MeV.

2.2. CATE-CsI(Tl) array

The CsI(Tl) array (see Fig. 2(d)) is placed about 40 mm behind the Si array in the CATE detector chamber to yield the residual energy, E_{res}, of the fragments. Each CsI(Tl) scintillator (model: $V52P25/18M-E2-\mathrm{Cs}-X(SSX848)$) [18] has a truncated pyramidal shape (see right-bottom part of Fig. 2(d)) with a base size of $(54 \times 54)\,\mathrm{mm}^2$, a minimal height of 10 mm and a maximal height of 25 mm. In 10 mm thickness all heavy ions with $Z \geqslant 7$ and $A \geqslant 14$ with an energy of $\leqslant 100$ A MeV are fully stopped [19]. For readout a photodiode with size of $(18 \times 18)\,\mathrm{mm}^2$ is attached at the smaller base, together with an integrated appropriate preamplifier [20]. The detectors are covered by 2 μm thick Mylar,[5] to protect the crystal, and to assure good light collection. All detectors are mounted in a very close geometry and separated in front by an Al holder frame, which covers a spacing of 4 mm between each two of them, thus reproducing the geometrical efficiency of the Si array.

---

[4] PIPS is a Trademark of Canberra.

[5] Mylar is a Trademark of DuPont.

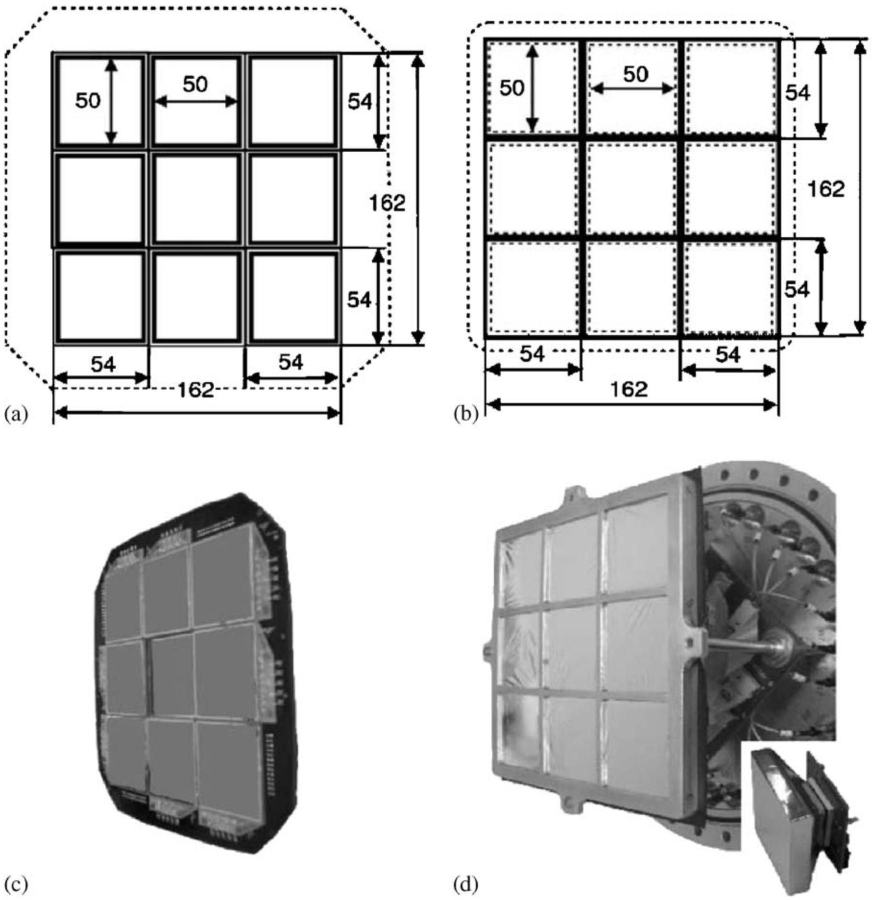

Fig. 2. Schematic representation of (a) the CATE-Si array and (b) the CATE-CsI(Tl) array; a photograph of (c) the CATE-Si array and (d) the CATE-CsI(Tl) array. A single CsI(Tl) detector is shown in the bottom-right corner.

The intrinsic energy resolution of the CsI(Tl) detectors was found to be about 0.7% (FWHM) for both a primary ^{86}Kr beam at an energy of 145 A MeV and for a ^{58}Ni beam at an energy of 113 A MeV.

3. Position sensitivity

The position, determined with the Si detectors gives a measure of the scattering angle of the particles, scattered off the RISING secondary target. The thickness of the secondary target is usually chosen to keep the angular straggling in the order of 10 mrad, corresponding to a position uncertainty at CATE of about 1 cm [2]. This value is not critical, compared to the beam spot size, and still allows suppression of the atomic background by selecting narrow forward angles.

The position in a Si detector is determined using the following algorithm:

$$x = \frac{D_x}{2} \frac{(q_B + q_C) - (q_A + q_D)}{q_A + q_B + q_C + q_D},$$
$$y = \frac{D_y}{2} \frac{(q_C + q_D) - (q_A + q_B)}{q_A + q_B + q_C + q_D} \qquad (1)$$

where q_A, q_B, q_C and q_D are the charges collected in the four corners A, B, C and D in Fig. 3(a), respectively. The used geometrical algorithm assumes that the co-ordinate system center is in the center of the active area, whose dimensions are D_x and D_y.

The algorithm is applied for the calculation of the two dimensional position with both Si detector types, and does not depend on the particle type and energy. However, due to the difference in the sheet resistance of the Si-IPP and Si-PIPS detectors, their performance differs as will be illustrated in the next sections.

3.1. Performance of CATE with Si-IPP detectors

The response of the CATE-Si array on ^{58}Ni particles with an energy of about 120 A MeV is shown in Fig. 3(b). As can be seen, the position reconstruction does not follow the real geometrical shape of the detectors and the spacings between them are not as in reality. The existing non-linearity deteriorates the position measurement, and is known as pin cushion effect [16]. This distortion of the position shape [17,21,22] for Si (2D-PSD) [14] detectors strongly depends on the resistivity of the resistive sheet, the

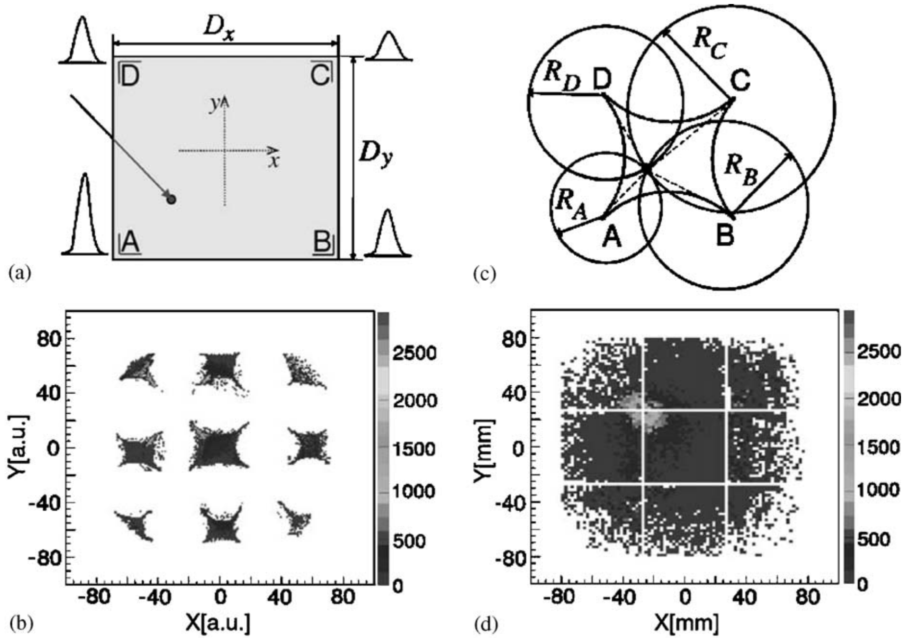

Fig. 3. Position determination (a) with a single Si-IPP detector; (b) initial position spectrum from the whole CATE Si-IPP array for ^{58}Ni particles with 120 A MeV; (c) schematic presentation of the $(1/R+\text{const})$ approximation for the position correction of a single Si-IPP detector; (d) corrected position spectrum of the whole CATE Si-IPP array, using the $(1/R+\text{const})$ approximation.

electrode termination resistors, the filter components of the preamplifier and the shaping time of the amplifier. Well developed correction methods [17,21,22] require knowledge of electronic details and separate current flow measurements not available for these detectors. Therefore, in order to correct the position response, a new linearization procedure has been developed.

3.2. Position corrections with Si-IPP detectors

To perform the position corrections, each detector is treated separately. The initial amplitude distributions of the four position signals (pins) are normalized to the back (sum) contact (A/E, B/E, C/E and D/E) in order to be able to disentangle the noise contributions from small amplitude signals due to interactions at the opposite corner. These new pin values are used for the reconstruction of the (x, y) position, calculated via Eq. (1). To symmetrize the obtained position shape, the normalized pin distributions are calibrated to each other, using a linear function, i.e. for pin A

$$A' = (A/E)\cdot \text{slope}_A + \text{offset}_A. \tag{2}$$

To normalize the symmetrized position shape to the real size of the Si-IPP detector, two new linear functions are constructed, acting in x and y directions

$$x'' = \text{blow}_x \cdot (x' + \text{offset}_x), \quad y'' = \text{blow}_y \cdot (y' + \text{offset}_y). \tag{3}$$

The $\text{blow}_{x,y}$ factors correct for the measured position squeezing and the $\text{offset}_{x,y}$ factors correct for the measured position offset. They are obtained from the projections on the x and y axes.

Further, it is assumed that all particles impinging at the same radial distance from a certain corner produce the same pulse height at that corner. This is valid for all other corners as well, and the position can be approximated with circles, whose four centers are the four corners, as demonstrated in Fig. 3(c). A simulation of the spectral response from a pin shows that the maximum radius ($R_{\max}$) achieved is equal to the size of the detector.

In this way, the position (x, y) becomes a function of the distance to each of the corners $f(R) = 1/(R + \text{const})$, namely

$$\begin{aligned} x &= c_1 \cdot c_2 \\ &\quad\times \frac{(1/R_A + c_1) + (1/R_D + c_1)}{(1/R_A + c_1) + (1/R_B + c_1) + (1/R_C + c_1) + (1/R_D + c_1)} \\ y &= c_1 \cdot c_2 \\ &\quad\times \frac{(1/R_B + c_1) + (1/R_C + c_1)}{(1/R_A + c_1) + (1/R_B + c_1) + (1/R_C + c_1) + (1/R_D + c_1)} \end{aligned} \tag{4}$$

where $1/R_A$, $1/R_B$, $1/R_C$ and $1/R_D$ are the distances to the corners A, B, C and D, respectively. The values of the two constants c_1 and c_2, utilized in Eq. (4), were determined empirically. The regular intensity distribution of the corrected position matrix leads to an estimated position uncertainty of $\leqslant 2$ mm with this simple approximation.

3.3. Performance of CATE with Si-PIPS detectors

The Si-PIPS type CATE detectors display a linear behavior of the measured position shape as can be seen in Fig. 4(a) for ^{58}Cr ions with an energy of about

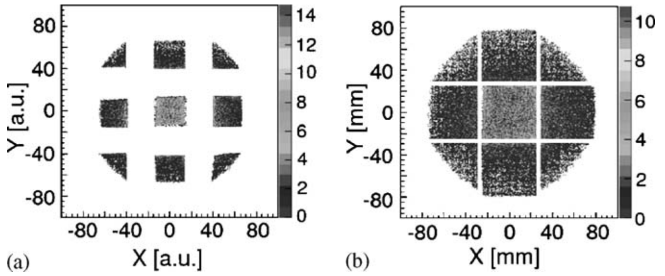

Fig. 4. (a) Raw and (b) corrected position from the CATE-Si PIPS detector array.

120 A MeV. Therefore, they do not need the correction procedure applied for the Si-IPP type. In order to expand the measured shape a simple calibration of the type presented in Eq. (3) is used. The corrected position matrix from the Si-PIPS array is plotted in Fig. 4(b).

4. The energy measurement and corrections

The energies detected in the CATE Si, ΔE, and CsI(Tl), E_{res}, detectors are used for the particle identification. Measured values are influenced by several effects: (i) the particle position, (ii) the beam velocity, (iii) the beam rate, (iv) the thickness of the secondary target, and (v) the reaction mechanism. The first effect is related to the nature of the detectors and their inhomogeneity, while the next two are effects related to the beam. The corrections can be done with well-defined primary beams and the intrinsic energy resolution of the detectors can be determined. The last two effects are typical for secondary beams. The target thickness chosen for an experiment is usually a compromise between the desired luminosity on one hand, and the still acceptable angular and energy straggling, on the other. Knock-out and fragmentation reactions are in addition associated with uncorrectable momentum spread (see Section 5.3). In general, the following corrections are applied:

(i) The effect of the particle impact position is observed as a centroid shift of the energies, determined by the CATE detectors, after applying a position condition to the Si (x, y) position matrix. This matrix is sub-divided into $(3 \times 3)\,\mathrm{mm}^2$ pixels. The correction is then done by aligning the energy for each of the pixels with respect to the central pixel. Thereby, the pixel correction factors are obtained by a calibration run using a primary beam well defined in energy, which is being swept across the active area of the detector.

(ii) The second effect, which is due to the particle momentum, is observed as a correlation between the detected energies with CATE and the velocity β, determined from the ToF, measured between the mid-section and the end of the FRS (see Fig. 1).

(iii) The high beam intensity and its distribution also influences the energy resolutions of the CATE detectors. When the particle rate at the detectors exceeds 10 kHz, an energy shift is observed in their spectral response towards low amplitudes. This effect is more strongly pronounced for the semiconductor detectors compared to the scintillators due to the time constant of their electronics.

(iv) The initial energy spread of the beam, observed by the variation of ToF, is amplified in the subsequent particle detectors and in the target. This effect is caused by the significant energy dependence of the energy loss in matter at around 100 A MeV. It can be corrected for, parametrizing this dependence as a function of β.

5. The particle identification

5.1. Charge (Z) determination

The atomic number, Z, is determined, as $\sqrt{\Delta E} \approx Z$ by measuring the energy loss ΔE in the Si detectors of CATE. It is approximated to be equal to the ion charge, q, at relativistic energies [1].

In all in-beam studies, the detector response revealed a unique Z identification. A typical example from secondary reactions of ^{55}Ni on a ^{9}Be target at 100 A MeV is depicted in Fig. 5(a). After a linearization, which is done by geometrical rotation around the main spot in the distribution and a calibration to the known incoming Z, the extracted resolution is $\Delta Z \approx 0.7$ (FWHM) (for $Z \in [18, 28]$). The typical spectrum in Z units can be seen in the insert of the figure.

Another example for the heavier system ^{112}Sn on ^{197}Au (see Fig. 5(b)), confirms the Z identification with resolution of $\Delta Z \approx 0.8$ (FWHM) (for $Z \in [30, 50]$). Thus, we conclude that the mean Z resolution from the out-coming particle cocktail is sufficient for the charge identification after the secondary target.

5.2. Mass (A) determination

The mass A of an impinging ion with a total energy, E_{tot}, can be determined using the relation $E_{\mathrm{tot}} \approx A \cdot \beta_A^2$. This holds if a constant velocity $\beta_A = \mathrm{const}$ for all ions is assumed. Combining the energy loss in the Si detectors, ΔE, with the energy, deposited in the CsI(Tl), E_{res}, the total energy of the ions $E_{\mathrm{tot}} = \Delta E + E_{\mathrm{res}}$ is obtained. After an error propagation, using the intrinsic energy resolutions of the CATE detectors the mass resolution $\Delta A/A$ is expected to be $\leqslant 1\%$. To achieve this value in the experimental data from secondary reactions corrections for all possible effects, described in Section 4, need to be done.

5.2.1. Coulomb excitation at the secondary target

The energy spread detected in CATE depends (i) on the straggling effects in the isotope production, the straggling

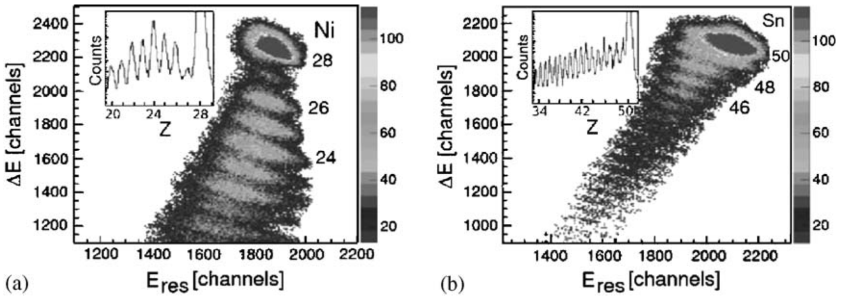

Fig. 5. $\Delta E-E_{\mathrm{res}}$ identification by CATE for the products from the reactions (a) ^{55}Ni on ^{9}Be target and (b) ^{112}Sn on ^{197}Au target. Spectra in Z units are shown in the inserts.

in the FRS tracking detectors, the straggling in the secondary target and the intrinsic resolution of the CATE detectors themselves; and (ii) on the isotope cocktail produced by neutron knock-out/fragmentation in the secondary target. In relativistic Coulomb excitation reactions, CATE is used to detect the same outgoing particles which impinge on the secondary target. Therefore, the incoming ions of interest are selected with the FRS identification detectors and no absolute energy calibration needs to be performed for the CATE detectors.

The mass resolution can be determined from the particle singles or from particle-γ events with very small scattering angles corresponding to atomic interactions because only the above mentioned "type (i)" effects are relevant. A typical reaction at an energy of about 170 A MeV is the system ^{53}V, ^{54}Cr and ^{55}Mn on ^{197}Au target. The $\Delta E-E_{\mathrm{res}}$ identification with CATE is similar to the one depicted in Fig. 5(b). To obtain the mass resolution in this case, a geometrical linearization by rotation of the distribution around the main spot is performed. After a Z selection from the linearized $\Delta E-E_{\mathrm{res}}$ distribution the deposited residual energy, E_{res}, is projected. The "mass" spectra with particle-γ coincidence condition for the three isotopes ^{53}V (top), ^{54}Cr (middle) and ^{55}Mn (bottom) are plotted in Fig. 6 with solid line. The nuclear reaction channels form in this case a wide distribution. Selecting a particle trigger condition pronounces the secondary beam-like residues, as depicted in Fig. 6 with dashed line. The mass resolution of CATE corresponds then to the width of these Coulomb excitation channels which is determined to be between 2 and 3% (FWHM).

5.2.2. *Fragmentation reactions at the secondary target*

In secondary fragmentation reaction (i.e. of ^{55}Ni particles as shown on Fig. 5(a)) CATE is used to identify each isotope produced in the secondary (^{9}Be) target to select the associated γ-ray spectrum. Therefore, an absolute calibration of the CATE detectors is performed using primary beam with well-defined energy and a small spot size.

5.2.3. *Linearization procedure*

To linearize the $\Delta E-E_{\mathrm{res}}$ distribution, following the formalism of Bethe [23], the power law method [24,25] is used. Its modifications and applicability [26–28] have been limited by the approximations made to the actual energy loss of the particles involved. Recently, a new method to treat the response of a $\Delta E-E$ telescope for charge, Z, and mass, A, identification has been developed by Tassan-Got [29] for the INDRA detector array [11]. With the help of energy functionals, an interpolation or extrapolation into regions with low statistics is allowed and have shown a good accuracy for relativistic particles, in comparison to identification functionals used in the past [24,26,28]. Therefore, these functionals have been preferred for the linearization of the CATE detector energies (ΔE and E_{res}).

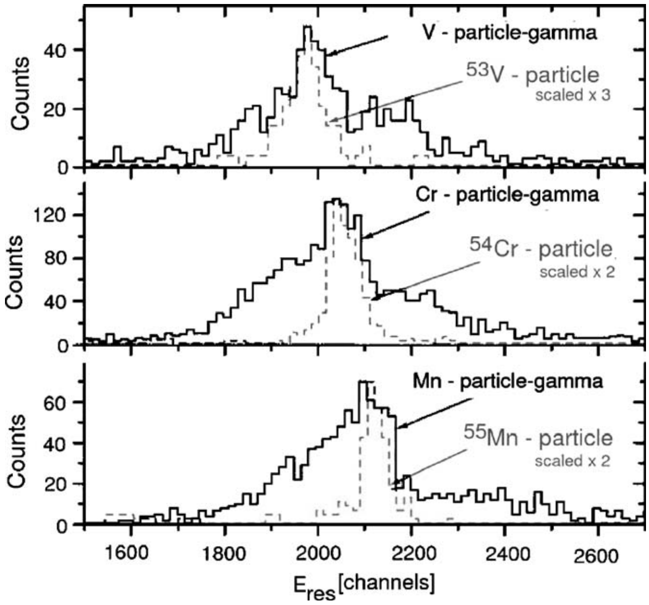

Fig. 6. Mass spectrum for the ^{53}V (top), ^{54}Cr (middle) and ^{55}Mn (bottom) isotopes with solid line for particle-gamma condition and with dashed line for particle singles.

The mass A of the particles is calculated

$$A=\left[\frac{(\Delta E+E)^{\mu+1}-(g\cdot E)^{\mu+1}}{\lambda^{\mu+1}Z^{2}}\right]^{1/\mu} \tag{5}$$

where the parameter g is the electronic gain ratio which in this case is the ratio between the slope coefficients from the energy calibration of the Si and the CsI(Tl) detectors: $g = a_{\Delta E}/a_{E_{\text{res}}}$; the parameter μ takes a typical value for the Bethe approximation of 0.7 [26,27]; the parameter λ is taken to be the absolute value of the ratio between the offsets from the energy calibration of the Si and the CsI(Tl) detectors respectively: $\lambda = |b_{\Delta E}/b_E|$.

The corresponding calculation of the mass difference ΔM is

$$\Delta M = E_{\text{tot}}^p - E_{\text{res}}^p \tag{6}$$

where the optimal parameter p for this specific data set is found to be 1.71.

A new function for the particle identification, PI_{dynamic}, is constructed, including the Z dependence of ΔM. The last is calculated for the observed charges $19 \leqslant Z \leqslant 28$ and fitted with a second order polynomial. In this way the particle identification function is calculated using

$$PI_{\text{dynamic}} = (Z(\Delta M) + w \cdot A - 2 \cdot Z(\Delta M))/k \tag{7}$$

where the optimal value of the parameter w is found to be $w = 0.4$ and k is a scaling coefficient. The identification of the different particles in terms of Z and A is then given by the correlation of the particle identification, PI_{dynamic}, as a function of the total energy, E_{tot}, deposited in the CATE detectors. The mass analysis is performed by selecting one of the parallel Z distributions from PI_{dynamic} and projecting it onto the total energy axis.

5.3. Mass resolution and comparison with simulations

One of the available ion-optical Monte Carlo simulation programs LISE [30] allows not only the calculation of the transmitted ions trough the FRS and its particle detectors but also precise energy loss calculations and realistic distributions. A comparison between a simulation using the LISE code [30] (see Fig. 7(a)) and the experimental data (see Fig. 7(b)) for the reaction ^{55}Ni on ^{9}Be target, demonstrates a good agreement. First review on this subject has been published in Ref. [31]. Contrary to the good charge identification, unique mass identification is not achieved. This is mainly caused by the reaction mechanism, leading to a broad momentum distribution which can not be corrected as the other effects described in Section 4. It has been explained by Goldhaber [32] as particle momentum widening due to the abrasion of nucleons, which leads a spread of the momentum or, respectively, the velocity of the final fragment. Therefore, the assumption of constant velocity for all secondary ion species does not hold. Consequently, without a time-of-flight measurement after the secondary target, the possible mass resolution is typically 2–3% (FWHM) at energies of about 100 A MeV.

A theoretical calculation of the single mass distributions, using the LISE code [30] was performed in order to compare and identify the experimental E_{tot} distribution, after an absolute energy calibration and linearization (see Section 5.2.3) [31]. As an illustration, the E_{tot} spectrum for $Z = 24$ isotopes is presented on Fig. 8(a) with multiple fit and deconvolution to single distributions (with reduced $\chi^2 \leqslant 15$; $\chi^2 = \chi^2/n$, where n is the number of degrees of freedom). The identification is performed by comparison of the energy centroids with the simulated single mass distributions. The experimental mass resolution is about 2–3% (FWHM).

5.4. Reaction channel selection by CATE

In Fig. 8(a) mass distributions for ^{49}Cr and ^{50}Cr are marked. In order to construct a particle-γ correlation, the particle-γ angle is calculated from particle angle after the secondary target, measured by CATE, and the γ-ray angle defined by the Ge detectors. This angle is used for the Doppler correction, applied to the measured, calibrated energy of all Ge detectors. The velocity of each isotope after the secondary target is calculated from the measured ToF and the energy losses in the experimental set-up. This velocity is normalized to the velocity, for each particular isotope, deduced after corrections from the total energy measured by the CATE detectors. Here these are the energy centroids of the mass distributions for ^{49}Cr and ^{50}Cr isotopes. The γ-spectra corresponding to these isotopes are obtained using particle tracking before and after the secondary target, from the calibrated and Doppler corrected Ge detector energies. Typically, additional conditions are applied to the time and multiplicity spectra of the Ge detectors. The channel selection by a CATE telescope is performed by selection of a single charge, Z, from the $PI_{\text{dynamic}}(E_{\text{tot}})$ identification and a single mass, A, from the projection to the E_{tot} axis (as demonstrated in the

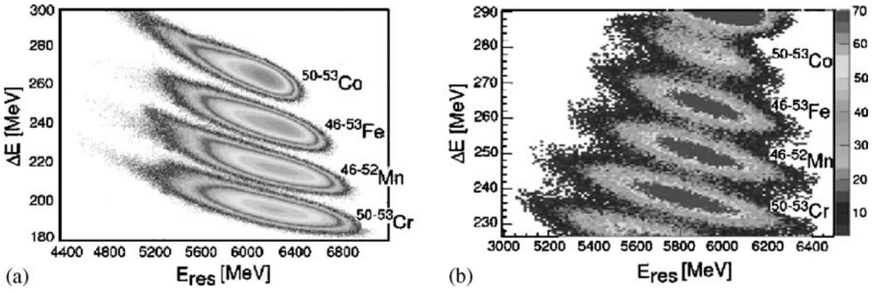

Fig. 7. Comparison between (a) a simulation and (b) the experimental data for the reaction ^{55}Ni on ^{9}Be target.

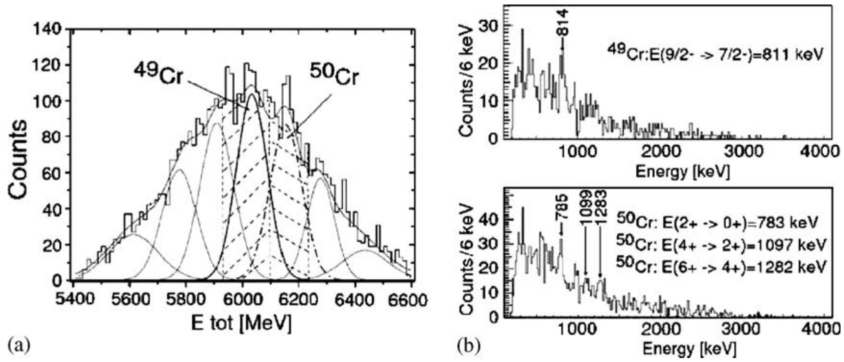

(a) (b)

Fig. 8. Measured (a) total energy spectrum (E_{tot}) for the ^{49}Cr (thick solid line) and ^{50}Cr (dash-dotted line) isotopes, produced in the reaction ^{55}Ni on ^{9}Be target. Measured (b) γ-spectra for the ^{49}Cr (top) and ^{50}Cr (bottom) isotopes [33].

figure). This is done because, as explained in Section 5.2.3, the $PI_{\mathrm{dynamic}}(E_{\mathrm{tot}})$ distribution is constructed so that it corresponds to the identification $Z(A)$. The observed γ-lines for ^{49}Cr are shown in Fig. 8(b) (top) and for ^{50}Cr in Fig. 8(b) (bottom). The observed γ-rays correspond to known transitions in these nuclei [33]. Their energies are indicated in Fig. 8(b). These lines can not be seen when applying only Z selection from CATE, which proves the importance of both Z and A identification after the RISING secondary target. The unidentified lines in the spectra originate from higher excited states and from remaining background in the Ge detectors.

6. Summary

With the newly developed $\Delta E - E_{\mathrm{res}}$ telescope, CATE, charge and mass identification of relativistic heavy ions at energies $\geqslant$100 A MeV can be performed. The system has a good position resolution $(\Delta x, \Delta y) \approx (3 \times 3)\,\mathrm{mm}^2$ for scattering angle reconstruction, a unique charge resolution ΔZ of 0.7 (FWHM) (for $Z \in [18, 28]$) and 0.8 (FWHM) (for $Z \in [30, 50]$) and a mass resolution of 1–3% (FWHM), limited by the target thickness for Coulomb excitation events, and 2–3% (FWHM) for fragmentation channels, further limited by the momentum broadening in the reaction. With an additional time-of-flight measurement of the outgoing particles the mass resolution for fragments could be improved to about 1% (FWHM).

References

[1] H. Geissel, et al., Nucl. Instr. and Meth. B 70 (1992) 286 ⟨www-wnt.gsi.de/frs/index.asp⟩.
[2] H.-J. Wollersheim, et al., Nucl. Instr. and Meth. A 537 (2005) 637 ⟨www-aix.gsi.de/~wolle/EB_at_GSI/rising.html⟩.
[3] J. Simpson, et al., Z. Phys. A 358 (1997) 139.
[4] J. Eberth, et al., Nucl. Instr. and Meth. A 369 (1996) 135.
[5] G. Marcazzan, et al., Nuovo Cimento 10 (1958) 155.
[6] D. Brayant, et al., IRE Trans. Nucl. Sci. NS-9 (3) (1962) 376.
[7] W. Wilcke, et al., Nucl. Instr. and Meth. 188 (1981) 293.
[8] S. Aiello, et al., Nucl. Phys. A 583 (1995) 461.
[9] F. Gramegna, et al., Nucl. Phys. A 389 (1997) 474.
[10] M. Simon, et al., Nucl. Instr. and Meth. A 452 (2000) 205.
[11] M. Parlog, etal., Nucl. Instr. and Meth. A 482 (2002) 674 and 693.
[12] S. Nageswara Rao, et al., Nucl. Instr. and Meth. B 111 (2003) 1.
[13] R. Lozeva, et al., Nucl. Instr. and Meth. B 204 (2003) 678.
[14] User's Manual for Si IPP-IPP 2D detectors, Eurisys Measures, 2001.
[15] PIPS Specification and performance sheet, Canberra Semiconductor Industries, 2004, ⟨www.canberra.com⟩, ⟨www.canberraeurisys.com⟩.
[16] T. Doke, et al., Nucl. Instr. and Meth. A 261 (1987) 605, and the references therein.
[17] R. Cowin, et al., Nucl. Instr. and Meth. A 399 (1997) 365.
[18] Scionix Co., 2004, ⟨www.scionix.nl⟩, ⟨www.scionixusa.com⟩.
[19] C. Scheidenberger, H. Geissel, Nucl. Instr. and Meth. B 135 (1998) 25 ⟨www-aix.gsi.de/~weick/atima/⟩.
[20] A. Pullia, et al., IEEE Trans. Nucl. Sci. NS-48 (3) (2001) 530.
[21] T. Yagimachi, et al., Nucl. Instr. and Meth. A 275 (1989) 307.
[22] M. Bruno, et al., Nucl. Instr. and Meth. A 311 (1992) 189.
[23] H. Bethe, Rev. Mod. Phys. 9 (1937) 69.
[24] F. Goulding, et al., Nucl. Instr. and Meth. 34 (1964) 1.
[25] F. Goulding, D. Landis, IEEE Trans. Nucl. Sci. NS-13 (1966) 514.
[26] G. Butler, et al., Nucl. Instr. and Meth. 89 (1970) 189.
[27] F. Goulding, B. Harvey, Ann. Rev. Nucl. Sci. 25 (1975) 167.
[28] T. Shimoda, et al., Nucl. Instr. and Meth. 165 (1970) 261.
[29] L. Tassan-Got, Nucl. Instr. and Meth. B 194 (2002) 503.
[30] O. Tarasov, D. Basin, Nucl Instr. and Meth. B 204 (2003) 174 ⟨dnr080.jinr.ru/lise⟩, ⟨groups.nscl.msu.edu/lise⟩.
[31] R. Lozeva, et al., Acta Phys. Pol. B 36 (2005) 1245.
[32] A. Goldhaber, et al., Phys. Lett B 53 (1974) 306.
[33] ENSDF database ⟨www.nndc.bnl.gov⟩.